Clays and Clay Minerals, Vol. 58, No. 6, 813–820, 2010.

ATOMIC FORCE MICROSCOPY METHOD FOR MEASURING SMECTITE COEFFICIENTS OF FRICTION

LAURA M. KOSOGLU[1], BARRY R. BICKMORE[2,*], GEORGE M. FILZ[1], AND ANDREW S. MADDEN[3]

[1] Department of Civil and Environmental Engineering, Virginia Tech, Blacksburg, VA 24061, USA
[2] Department of Geological Sciences, Brigham Young University, Provo, UT 84602, USA
[3] School of Geology and Geophysics, University of Oklahoma, Norman, OK 73019, USA

Abstract—The coefficient of friction of clay minerals at the micro-scale has generally not been studied due to difficulties in obtaining measurements in a bulk-soil volume undergoing shear at such small scales. Information on friction at the micro-scale may provide insight into grain-scale processes that operate in bulk samples or in natural faults. The objective of this study was to develop a method to measure the micro-scale friction coefficient of smectites. The experiments described show that the axial atomic force microscopy method can be adapted to easily obtain accurate coefficient of friction (μ) measurements for smectites from force curves involving colloidal probes. The method allows for the measurements to be performed over spatial scales of a few μm, can be carried out under dry conditions or a wide range of aqueous solutions, and requires no calibration beyond making a few microscopic measurements of the probe. This method provides measurements of micro-scale normal and shear forces between minerals, which can be used for a variety of applications such as the study of shear deformation, consolidation, and fault dynamics. Control tests of silica on mica (μ = 0.29±0.02) agree with literature values where limits indicate one standard deviation. Coefficient of friction values for wet and dry Na-montmorillonite were determined to be 0.20±0.03 and 0.72±0.03, respectively.

Key Words—AFM, Coating, Creep, Force, Friction, Montmorillonite, Probe, SWy-2.

INTRODUCTION

The coefficient of friction (μ) is defined as the ratio of the tangential force (F_T) to the normal force (F_N) between two objects in contact.

$$\mu = \frac{dF_T}{dF_N} \quad (1)$$

The value of μ is independent of surface roughness and contact area but is dependent on the type of materials in contact and external conditions such as humidity (Gao *et al.*, 2004).

The design of building foundations often requires the calculation of the macro-scale compression of clay minerals over time. Mechanical loading of water-saturated clays results in compression due to the transfer of stress from the water phase to the solid phase associated with hydrodynamic expulsion of water from the clay, known as primary consolidation. Volume changes can also result from the continuing adjustment and breakage of clay particles, which can occur under constant effective stress and is termed secondary compression. Typically the parameters defining the rate of primary consolidation and secondary compression are determined from laboratory tests on representative samples of the clay. Based upon these lab results, expected settlement of a proposed construction can be estimated (Lambe and Whitman, 1969).

The μ of minerals also plays a fundamental role in the study of fault dynamics. The behavior and shear strength of discontinuities in geological masses vary as a function of the residual friction angle (Price, 2009). The residual friction angle is related to the resistance of the failed shear surface after considerable movement. μ is also used to determine the angle at which a fault should form (Bunds, 2001). A range of earthquake phenomena have been explained based upon time-dependent 'rate and state' friction laws that incorporate empirical parameters, often considering both field data and laboratory rock-friction experiments (*e.g.* Scholz, 1998).

Multiple lines of evidence suggest that the strength of many faults is significantly weaker than would be expected based on the friction values determined for rocks in laboratory experiments (*e.g.* Zoback, 2000; Holdsworth, 2004), although multiple hypotheses continue to be tested (*e.g.* Zoback *et al*., 2010).

The presence of relatively weak minerals such as phyllosilicates with small μ values may contribute to overall fault weakness. Fine-grained broken and chemically altered gouge material along the active traces of faults often contains clay minerals (*e.g.* Wu *et al*., 1975; Solum *et al*., 2006; Schleicher *et al*., 2009; Solum *et al*., 2009), and experimental evidence suggests that large volume percentages or localized concentrated zones of clay minerals might be required to account for field observations (*e.g.* Tembe *et al*., 2006; Carpenter *et al*., 2009). Detailed observations of materials from depth in an

* E-mail address of corresponding author:
barry_bickmore@byu.edu
DOI: 10.1346/CCMN.2010.0580609

actively creeping section of the San Andreas fault (the San Andreas Fault Observatory at Depth or SAFOD project, Zoback *et al*., 2010) led to a variety of relevant findings. Talc, known to have extremely small μ values, was discovered in cuttings of serpentinite from rocks that are believed to be currently creeping (Moore and Rymer, 2007). In addition, localized <100 nm thick coatings of several clay minerals, including illite-smectite and chlorite-smectite, crystallized relatively recently (~4–8 Ma) on the surfaces of gouge grains (Schleicher *et al*., 2010). These observations present the possibility that networks of low-friction phyllosilicates could be responsible for weakening of the San Andreas and other faults (*e.g.* Kopf and Brown, 2003; Colletini *et al*., 2009). Another complication is that while laboratory experiments and modeling suggest that the μ value of phyllosilicates is smallest when the preferred orientation of the basal planes is maximized (*e.g.* Wintsch *et al*., 1995; Kock and Huhn, 2007; Collettini *et al*., 2009), field studies suggest that clay fabrics are not oriented except perhaps at very localized scales (*e.g.* Solum *et al*., 2009; Wenk *et al*., 2010). In all these cases, friction measurements of smectite and mixed-layer clay minerals can contribute to the evolving understanding of fault slip.

These applications of μ consider friction as a macro-scale phenomenon. The value of μ is often scale-independent (Gao *et al*., 2004), but this is not always the case. For example, Kuhn and Mitchell (1993) provided evidence that clay creep may be controlled at the molecular scale by the arrangement of silica tetrahedra rather than by the macro-scale surface roughness of the clay particles. Similarly, Dieterich and Kilgore (1994) attributed frictional forces in rocks to small-scale forces operating at contact points. However, no method was available at that time to measure μ at microscopic scales.

This issue may now be addressed *via* atomic force microscopy (AFM). The technology has long been used to image clay-particle morphology (*e.g.* Blum, 1994; Bosbach *et al*., 2000; Bickmore *et al*., 2001, 2002; Piner *et al*., 2003) and has even been used to measure the pore structure of wet clay (Selvam *et al*., 2006). Nishimura *et al.* (2002) used the AFM colloidal probe technique to measure normal forces between the basal surfaces of a synthetic smectite, and AFM has also been used to measure micro-scale frictional forces by tracking the torsion of the cantilever during scanning (*e.g.* Ruan and Bhushan, 1994; Bhushan *et al*., 1995; Jones *et al*., 2004; Gao *et al*., 2004; Bhushan, 2005; Gnecco *et al*., 2005). However, the latter technique requires painstaking calibration of both the torsional spring constant of the cantilever and the lateral sensitivity of the photodetector.

Attard and coworkers (*e.g.* Stiernstedt *et al*., 2005; Attard *et al*., 2007) recently developed an ''axial'' method for extracting μ values from AFM colloidal probe force curves. All that is required is precise measurement of the probe and cantilever dimensions, and no other calibration is necessary. The adaptation of this method to measure the μ value of a smectite is described here. Not only does the technique provide excellent estimates of μ, but one can easily use it to measure changes in both frictional and normal forces under widely varying solution conditions.

MATERIALS AND METHODS

In order to apply the technique to clay minerals: (1) suitable AFM probes were manufactured and characterized; (2) probes and substrates were coated with smectite, and (3) AFM force curves were obtained and analyzed to obtain wet and dry μ values for smectite. Each of these steps is described below.

AFM probe manufacture and characterization

Standard AFM tips are relatively sharp with a probe-tip diameter on the order of 20 nm and a height of 20 μm. These sharp tips are useful for imaging purposes, but they are not ideal for force measurements. The contact area of the tip is often irregularly shaped, which makes the effective radius of curvature difficult to determine. In addition, the contact area of a standard, sharp AFM tip is relatively small, which can result in unacceptably low signal-to-noise ratios in force measurements. Finally, a sharp tip is easy to damage when conducting friction measurements.

To mitigate the problems associated with using standard AFM tips for friction measurements, custom AFM probes were produced in house. These probes consisted of silica glass micro-spheres 50 μm in diameter (Corpuscular Inc., Cold Spring, New York) glued to the ends of tipless AFM cantilevers (Mikromasch USA, San Jose, California, series NSC12 or CSC12, Al-coated).

A cantilever was chosen from each NSC12 or CSC12 chip, with a length varying from 96 to 130 μm. The micro-spheres were shipped in deionized water. To make the micro-spheres accessible to the AFM, a piece of trimmed-to-size, freshly cleaved muscovite was epoxied to an AFM sample puck and heated on a hotplate at 100ºC. The vial containing the micro-spheres was shaken by hand, and a pipette was used to extract 50 μL from the vial and to drop the suspended micro-spheres onto the heated puck to dry. The puck was then allowed to cool.

The AFM probes were assembled using the following procedure. The AFM chip and chip holder were first cleaned in a UV/ozone cleaner (BioForce Nanosciences, Ames, Iowa, USA) for 20 min to remove organic-surface contaminants. A second muscovite puck was made, and then the AFM chip in the chip holder and the puck were loaded into the AFM. The cantilever of interest was located using the AFM optical microscope, and a small amount of mixed Loctite™ Marine Epoxy was dabbed onto the muscovite using a plastic toothpick. Using the

https://doi.org/10.1346/CCMN.2010.0580609 Published online by Cambridge University Press

AFM as a micromanipulator, the cantilever of interest was moved over the glue spot and lowered onto the glue. Care was taken so that only the very tip of the free end of the cantilever touched the epoxy and that the cantilever was lowered slowly to prevent it from crashing into the muscovite and bending excessively. Once the end of the cantilever was coated in wet epoxy, the tip was raised sufficiently to allow removal of the muscovite puck. The micro-sphere-coated muscovite puck was then loaded quickly into the AFM, and a lone micro-sphere was located using the AFM optical microscope. The glue-coated tip of the cantilever was lowered slowly onto the center of the micro-sphere. Once contact was made, the cantilever was raised slowly, and the micro-sphere was attached to the probe. The chip was removed from the AFM chip holder and placed in a numbered grid gel case. The glue was allowed to solidify for 24 h to ensure a strong bond prior to friction measurements.

The dimensions of the probes were characterized using an Environmental Scanning Electron Microscope (ESEM) (Philips XL30 ESEM-FEG, FEI Company, Hillsboro, Oregon, USA). Figure 1a shows an ESEM image of one of the probes, and Figure 1b shows a diagram of a probe marked to illustrate the dimensions measured. L_0 is the flexible length of the cantilever from the base to the edge of the glue spot holding the glass sphere, and L_1 is the distance from the edge of the glue spot to the point on the cantilever at which the sphere is attached. L_2 is the diameter of the sphere. One must also obtain the angle θ between the cantilever and the horizontal from the AFM manufacturer specifications ($\theta < 0$). This angle can be estimated as ~−10 to −15º in most cases (Attard *et al.*, 1999, 2007).

The μ measurements described here require no calibration other than the probe dimensions just discussed and the θ angle. Measurements of normal forces between the probe and sample, however, depend on the normal spring constant of the cantilever. The normal spring constants of each cantilever was measured before attachment of the micro-sphere probe *via* the thermal method with a Dimension 3100 AFM (Veeco, Santa Barbara, California, USA) with closed-loop scanning capability. A closed-loop scanner is necessary for this method and provides much greater precision in collecting force curves.

Attard *et al.* (2007) explained that the calibrated spring constant (k_{cal}) obtained must be corrected for the modifications made to the probe and the angle of approach (θ). The effective spring constant (k_{eff}) is calculated using equation 2 (Attard *et al*., 2007).

$$k_{eff} = \frac{k_{cal}}{\cos^2\theta}\left(\frac{L_{cal}}{L_0}\right)^3 \quad (2)$$

L_{cal} is the full length of the cantilever (which was also measured with the ESEM) when the thermal method is used to obtain k_{cal}.

Clay-coating AFM probes

The reference smectite SWy-2 (obtained from the Source Clays Repository of The Clay Minerals Society) was Na^+-saturated, centrifuged, and oven dried to obtain the <2 μm fraction. Information on how to calculate the centrifuge time needed for a given size cutoff using Stokes' Law was provided by Svedberg and Nichols (1923). To attach a layer of clay to both the micro-sphere

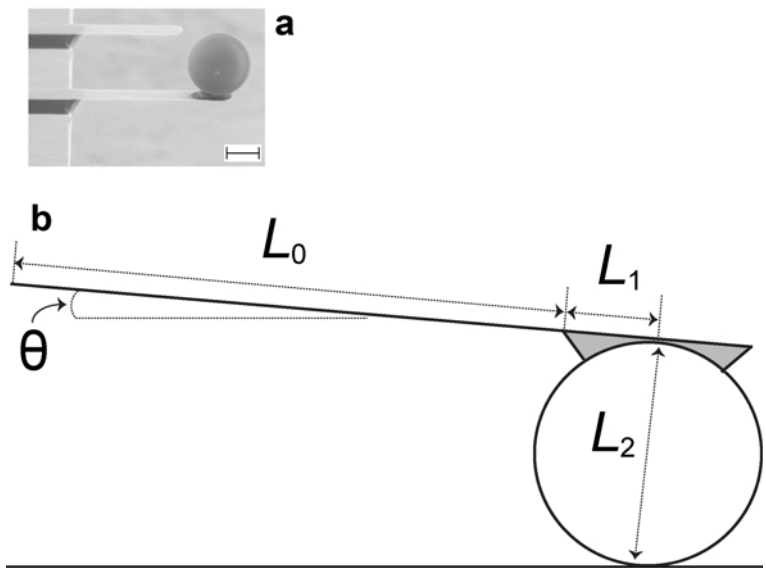

Figure 1. (a) ESEM image of a 52 μm-diameter glass micro-sphere glued to a cantilever (scale bar = 25 μm). (b) AFM probe geometry parameters (adapted from Attard *et al.*, 2007) needed to extract μ values from force curves.

https://doi.org/10.1346/CCMN.2010.0580609 Published online by Cambridge University Press

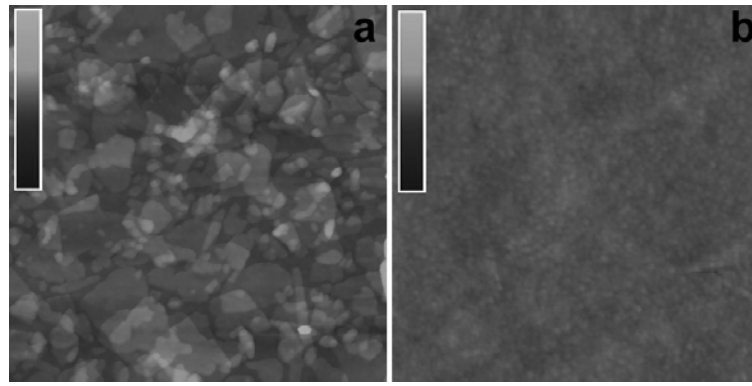

Figure 2. 2 μm × 2 μm AFM images of (a) a glass slide covered with SWy-2 particles (topographic scale = 20 nm), and (b) a glass slide (topographic scale = 10 nm).

probe and a sample substrate, the procedure developed by Bickmore *et al.* (1999) was used. A glass coverslip was epoxied onto an AFM sample puck. Polyethyleneimine $(C_2H_5N)n$, PEI (M.W. 1800, Polysciences, Warrington, Pennsylvania, USA), was diluted 1:2000 by mass with deionized water. The puck was then cleaned in the UV/ozone cleaner for 20 min, immersed in the PEI solution for 30 s, rinsed continuously with deionized water for 5 min, oven-dried for 1 h, and allowed to cool. A 0.1 g/L clay mineral dispersion was prepared using a sonic dismembrator for 10 min. After heating the puck on a hotplate to >100ºC, 100 μL of the clay dispersion was pipetted onto the heated puck and left for 1 min to flash boil the clay onto the mica substrate. The puck was then rinsed continuously with deionized water for 20 s and dried with compressed air. Finally, the coated puck was cleaned in the UV/ozone cleaner for 20 min. The coating coverage was verified with the AFM in tapping mode using a standard Si tip to obtain three-dimensional topographic images, which were compared to images taken of the plain silica glass (Figure 2). No attempt was made to measure the coating thickness, however.

A similar procedure was used to coat the AFM spherical glass probes with SWy-2, but modified slightly because of the small size of the AFM probe. The AFM chip was put into the AFM fluid chip holder and cleaned in the UV/ozone cleaner for 20 min. The AFM chip was then removed from the chip holder using tweezers and submerged into a small beaker containing the same PEI dilution for 30 s. After this step, the chip was immersed into a second beaker containing deionized water and held with tweezers in the water for 5 min. The chip was not allowed to drop into either beaker given the delicate probe on the end. After returning the chip to the fluid chip holder, the chip was oven-dried for 1 h and allowed to cool. A more concentrated, 1.0 g/L dispersion was made by mixing the clay in deionized water and dispersing with the sonic dismembrator for 10 min. The chip was then removed from the chip holder and held for 30 s in the clay dispersion using tweezers before immersing it for 2 min in deionized water in a second beaker. The chip was then placed back into the fluid chip holder, oven-dried for 5 min, and allowed to cool. An optical microscope was used to verify that the microsphere was still attached to the cantilever. Finally, the AFM chip was put into the AFM chip holder and cleaned in the UV/ozone cleaner for 20 min.

Micro-scale clay coefficient of friction measurements

In the method of Attard and coworkers (*e.g.* Stiernstedt *et al.*, 2005; Attard *et al.*, 2007), μ estimates are extracted from deflection-distance curves. One can obtain force-separation curves from these data, given an estimate of k_{eff} (Figure 3), but, if given a sufficiently large spherical probe, one can also obtain μ estimates from the hysteresis in the constant compliance region of the data (Figure 4). This hysteresis occurs because the probe approaches the sample surface at an angle (θ). When the probe touches the surface, the cantilever

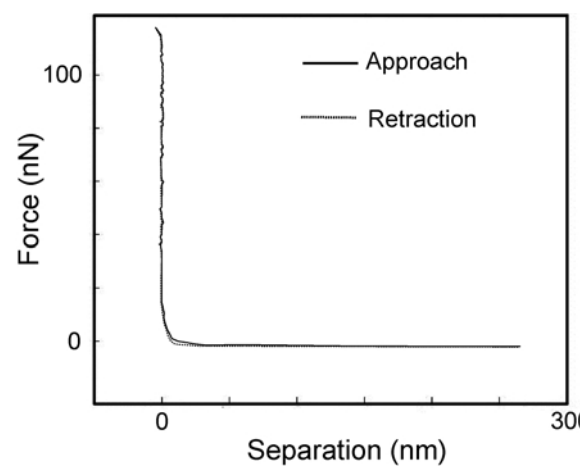

Figure 3. Force *vs*. separation on approach and retraction of the AFM probe for a glass sphere on mica. The maximum normal force applied was 115 nN.

https://doi.org/10.1346/CCMN.2010.0580609 Published online by Cambridge University Press

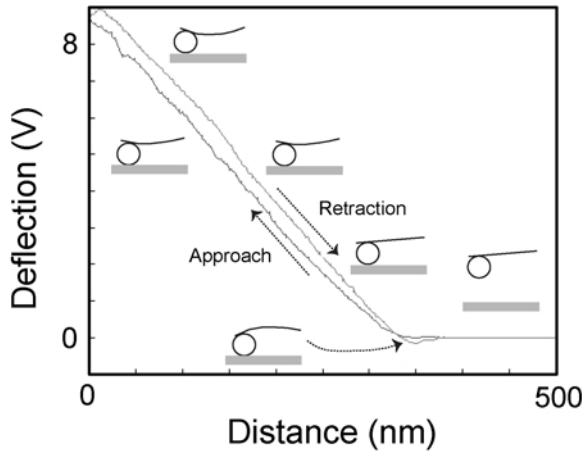

Figure 4. Deflection *vs*. distance curve for smectite shearing on smectite in a wet environment. Schematics of cantilever deflection are greatly exaggerated for explanatory purposes.

bends, causing the probe to rotate and slide. The rotation and sliding are impeded by frictional forces, resulting in hysteresis between the constant compliance regions of the approach and retraction curves. Attard and co-workers (*e.g.* Stiernstedt *et al.*, 2005; Attard *et al.*, 2007) derived the equations that provide the value of μ in terms of L_0, L_1, L_2, θ, and the difference in slope between the constant compliance regions of the approach and retraction curves. The sliding velocity during the tip-sample interaction can also be calculated from these parameters and the approach and retraction velocities.

The reader should consult Stiernstedt *et al.* (2005) for a complete derivation and explanation of the equations used to calculate μ and the sliding velocity. One of the authors (B.R. Bickmore) has created a *MatLab* program with a graphical user interface to extract μ values and sliding velocity values from force curves. The program could easily be modified to load force curves from any AFM vendor and is available from the author on request. The program also uses equation 2 to calculate k_{eff} and converts deflection-distance curves to force-separation curves.

Attard *et al*. (2007) tested their new axial method for measuring μ against the standard lateral method. They measured the wet μ of silica glass on mica as 0.27±0.01 (36 μm diameter silica glass probe, axial method), 0.29±0.03 (16 μm diameter silica glass probe, axial method), and 0.31±0.01 (36 μm diameter silica glass probe, lateral method) where limits indicate the standard error on the mean. The results show that the two methods provide comparable results.

341 force curves were collected using the clay-coated probes and samples in 0.001 M NaCl solution in the AFM fluid cell and 74 force curves under atmospheric conditions (dry). Different probes were used for the wet and dry tests. The wet friction tests were conducted at four different locations on the substrate, and the dry friction tests were conducted at two different locations on the substrate. The μ values did not appear to change over time during testing.

RESULTS AND DISCUSSION

Control tests

Several control tests were conducted to ensure that the procedure described in this paper generated accurate μ values. Atomic force microscope friction experiments were conducted to determine the wet μ values of silica glass on mica. Based on these experiments, μ = 0.29±0.02 (limits always indicate one standard deviation in this study's results), which matches well with the values determined by Attard *et al*. (2007) of 0.26 to 0.32 using both the axial and lateral methods.

Another control test was conducted to ensure that potential leftover PEI (used to glue clay particles to the probe) was removed using the UV/ozone cleaner. Remaining PEI would stick to the opposing surface and lead to erratic behavior and erroneously large μ values. Friction experiments were conducted before the PEI was applied, after the PEI was applied, and after the PEI was removed. The results (Table 1) show that the UV/ozone cleaner removed excess PEI effectively.

The final control test was to ensure that the UV/ozone cleaning process did not negatively affect the clay coverage. The smectite-coated substrates were imaged before and after cleaning, rinsing with DI water, and drying (Figure 5). The topographic scans before and after cleaning show that the cleaning procedure did not adversely affect clay coverage of the substrate.

Experiments

The wet Na-montmorillonite μ value was determined to be 0.20±0.03. These results are in quantitative agreement with the macro-scale residual μ values of 0.07−0.18 reported by Mitchell and Soga (2005) for Na-montmorillonite and the macro-scale wet μ value of 0.21 reported by Moore and Lockner (2004) for smectite. In the present study, the sliding velocity between the two surfaces in wet tests was ~1 μm/s, and the maximum applied normal force was ~800 nN in each test. Velocity and force variations were negligible. The dry μ value was also measured for montmorillonite as 0.72±0.03,

Table 1. PEI control test results. After application of PEI, the μ value of the probe sample is much greater, but returns to its original value after UV/ozone cleaning.

	Wet μ
Before PEI application	0.29±0.01
After PEI application	0.47±0.02
After UV/ozone cleaning	0.28±0.01

https://doi.org/10.1346/CCMN.2010.0580609 Published online by Cambridge University Press

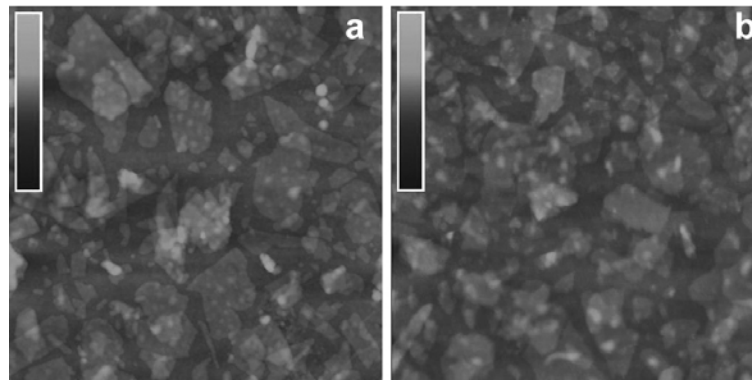

Figure 5. 2 μm × 2 μm AFM images of clay coverage (a) before and (b) after UV/ozone cleaning (topographic scale = 20 nm).

which is in quantitative agreement with the macro-scale dry μ value of ~0.7 measured by Morrow *et al.* (1982) and Moore and Lockner (2007). The sliding velocity between the two surfaces in the dry tests was varied from 0.1−0.5 μm/s, and the maximum applied normal force was ~180 nN in each test.

The close correlation observed between macro- and micro-scale μ measurements may contribute to a better understanding of the main factors controlling friction between smectite particles. Moore and Lockner (2004) showed that both the wet and dry μ values of 2:1 phyllosilicates generally follow very well defined trends with respect to certain crystallochemical factors. The wet μ values correlate fairly well with the electrostatic separation energy of the layers (Giese, 1978, 1980; Bish and Giese, 1981), and exceptionally well with the amount of tetrahedral layer charge. The dry μ values are exceptionally well correlated with the electrostatic separation energy of the layers. These observations lend support to the idea that friction between phyllosilicate layers is, indeed, controlled by molecular-scale factors (Kuhn and Mitchell, 1993). While the correlation of Moore and Lockner (2004) between dry μ values and electrostatic separation energy predicts $\mu \approx 0.4-0.5$ for smectites, the measured values are much larger ($\mu \approx 0.7$), thus suggesting that non-molecular-scale factors may be controlling the friction of smectites under dry conditions. Even though such factors have yet to be identified, they clearly can involve characteristic distances no greater than the few μm represented by the contact area of the micro-sphere probes and sample surfaces.

One possible solution to this problem involves the tendency of drying smectites to form particles less than a few μm across. Smectites are unique among 2:1 phyllosilicates, in that under certain conditions (*e.g.* Na^+-saturated smectite interlayers and small ionic strength) the individual layers may completely disperse in water. When such a dispersion is dried, the layers may come back together in a somewhat haphazard fashion. While the layers preferentially aggregate face-to-face along their basal surfaces, they may be misaligned horizontally, have different sizes, and so on. As the individual platelets are quite flexible, they bend to fit their surroundings, with the result that the aggregates often form in a shape more like an American football than a deck of cards. The frictional strength of most minerals follows Byerlee's Law, *i.e.* $\mu \approx 0.85$, but phyllosilicates are a major exception to the rule, ostensibly because of the parallel planes of weaker bonds between layers (Moore and Lockner, 2004). If the orientations of smectite layers in dried samples are sub-parallel, their frictional strength may be related to more than just the ease with which individual layers can slide past one another, and their overall behavior may more closely approximate Byerlee's Law. The extremely large range for montmorillonite μ values in macro-scale experiments (0.06−0.78, Moore and Lockner, 2007) could perhaps be explained by variable hydration state, pore pressures, and variability in the thickness and geometry of particles formed during drying. In natural systems such as soils and fault gouges, textural relations among material components and in relation to the stress field would probably contribute to a variety of initial or 'static' friction coefficients. Once deformation begins, grains may align to give smaller values of 'dynamic' or 'steady-state' friction, although at least for montmorillonite the development of preferred orientation textures also depends on the hydration state (*e.g.* Moore and Lockner, 2004). Alignment of grains would then potentially reduce the shear strength of the material. Certainly this explanation is speculative at this point, but it serves to illustrate how friction measurements at multiple spatial scales might prove useful.

CONCLUSIONS

The axial AFM method of Attard and coworkers (*e.g.* Stiernstedt *et al.*, 2005; Attard *et al.*, 2007) was adapted to easily obtain accurate coefficient of friction (μ) measurements for smectites. Using this method, measurements can be performed over spatial scales of a few

https://doi.org/10.1346/CCMN.2010.0580609 Published online by Cambridge University Press

μm, can be done under dry conditions or in various aqueous solutions, and require no calibration beyond measuring the AFM probe dimensions. This technique may also be adaptable to other very fine-grained clay materials and to fault gouge. Using this technique, control tests of silica on mica ($\mu = 0.29 \pm 0.02$) agree with literature values. Coefficient of friction values for wet and dry Na-montmorillonite were determined to be 0.20 ± 0.03 and 0.72 ± 0.03, respectively.

ACKNOWLEDGMENTS

The information presented here is based on work supported, in part, by the U.S. National Science Foundation under grant No DGE-0504196. Any opinions, findings, conclusions, and recommendations in this paper are those of the authors and do not necessarily reflect the views of the U.S. National Science Foundation. The authors acknowledge the assistance and advice of Michael F. Hochella, Jr., of the Geosciences Department at Virginia Tech in the preliminary stages of this research. BRB thanks the National Science Foundation (EAR-0525340) for supporting his part in this work. ASM thanks Ze'ev Reches for helpful discussions. Diane Moore, Faïza Bergaya, and an anonymous reviewer provided helpful comments on the original manuscript.

REFERENCES

Attard, P., Carambassis, A., and Rutland, M.W. (1999) Dynamic surface force measurement. 2. Friction and the atomic force microscope. *Langmuir*, **15**, 553–563.

Attard, P., Stiernstedt, J., and Rutland, M.W. (2007) Measurement of friction coefficients with the atomic force microscope. *Journal of Physics: Conference Series*, **61**, 51–55.

Bhushan, B. (2005) Nanotribology and nanomechanics. *Wear*, **259**, 1507–1531.

Bhushan, B., Israelachvili, J.N., and Landman, U. (1995) Nanotribology – friction, wear and lubrication at the atomic-scale. *Nature*, **374**, 607–616.

Bickmore, B.R., Hochella, M.F., Bosbach, D., and Charlet, L. (1999) Methods for performing atomic force microscopy imaging of clay minerals in aqueous solutions. *Clays and Clay Minerals*, **47**, 573–581.

Bickmore, B.R., Bosbach, D., Hochella, M.F., Jr., Charlet, L., and Rufe, E. (2001) In situ atomic force microscopy study of hectorite and nontronite dissolution: Implications for phyllosilicate edge surface structures and dissolution mechanisms. *American Mineralogist*, **86**, 411–423.

Bickmore, B.R., Nagy, K.L., Sandlin, P.E., and Crater, T.S. (2002) Quantifying surface areas of clays by atomic force microscopy. *American Mineralogist*, **87**, 780–783.

Bish, D.L. and Giese, R.F., Jr. (1981) Interlayer bonding in IIb chlorite. *American Mineralogist*, **66**, 1216–1220.

Blum, A.E. (1994) Determination of illite/smectite particle morphology using scanning force microscopy. Pp. 171–202 in: *Scanning Probe Microscopy of Clay Minerals* (K.L. Nagy and A.E. Blum, editors). Workshop Lecture Series, **7**, The Clay Minerals Society, Boulder, Colorado, USA.

Bosbach, D., Charlet, L., Bickmore, B.R., and Hochella, M.F., Jr. (2000) The dissolution of hectorite: In-situ, real-time observations using atomic force microscopy. *American Mineralogist*, **85**, 1209–1216.

Bunds, M.P. (2001) Fault strength and transpressional tectonics along the castle mountain strike-slip fault, southern Alaska. *Geological Society of America Bulletin*, **113**, 908–919.

Carpenter, B.M., Marone, C., and Saffer, D.M. (2009) Frictional behavior of materials in the 3D SAFOD volume. *Geophysical Research Letters*, **36**, L05302.

Collettini, C., Viti, C., Smith, S.A.F., and Holdsworth, R.E. (2009) Development of interconnected talc networks and weakening of continental low-angle normal faults. *Geology*, **85**, 567–570.

Dieterich, J.H. and Kilgore, B.D. (1994) Direct observation of frictional contacts; new insights for state-dependent properties. *Pure and Applied Geophysics*, **143**, 283–302.

Gao, J.P., Luedtke, W.D., Gourdon, D., Ruths, M., Israelachvili, J.N., and Landman, U. (2004) Frictional forces and Amontons' law: From the molecular to the macroscopic scale. *Journal of Physical Chemistry B*, **108**, 3410–3425.

Giese, R.F., Jr. (1978) The electrostatic interlayer forces of layer structure minerals. *Clays and Clay Minerals*, **26**, 51–57.

Giese, R.F., Jr. (1980) Hydroxyl orientations and interlayer bonding in amesite. *Clays and Clay Minerals*, **28**, 81–86.

Gnecco, E., Bennewitz, R., Pfeiffer, O., Socoliuc, A., and Meyer, E. (2005) Friction and wear at the nanoscale. Pp. 484–532 in: *Nanotribology and Nanomechanics* (B. Bhushan, editor). Springer, Berlin.

Holdsworth, R.E. (2004) Weak faults – rotten cores. *Science*, **303**, 181–182.

Jones, R., Pollock, H.M., Geldart, D., and Verlinden-Luts, A. (2004) Frictional forces between cohesive powder particles studied by AFM. *Ultramicroscopy*, **100**, 59–78.

Kock, I. and Huhn, K. (2007) Influence of particle shape on the frictional strength of sediments – a numerical case study. *Sedimentary Geology*, **196**, 217–233.

Kopf, A. and Brown, K.M. (2003) Friction experiments on saturated sediments and their implications for the stress state of the Nankai and Barbados subduction thrusts. *Marine Geology*, **202**, 193–210.

Kuhn, M.R. and Mitchell, J.K. (1993) New perspectives on soil creep. *Journal of Geotechnical Engineering*, **119**, 507–524.

Lambe, T.W. and Whitman, R.V. (1969) *Soil Mechanics*. John Wiley & Sons, Inc., New York.

Mitchell, J.K. and Soga, K. (2005) *Fundamentals of Soil Behavior*. John Wiley & Sons, Inc., New Jersey, USA.

Moore, D.E. and Lockner, D.A. (2004) Crystallographic controls on the frictional behavior of dry and water-saturated sheet structure minerals. *Journal of Geophysical Research*, **109**, 1–16.

Moore, D.E. and Lockner, D.A. (2007) Friction of the smectite clay montmorillonite: A review and interpretation of data. Pp. 317–345 in: *The Seismogenic Zone of Subduction Thrust Faults* (T.H. Dixon and C. Moore, editors). MARGINS Theoretical and Experimental Earth Science Series, Vol. 2, Columbia University Press, New York.

Moore, D.E. and Rymer, M.J. (2007) Talc-bearing serpentinite and the creeping section of the San Andreas fault. *Nature*, **448**, 795–797.

Morrow, C.A., Shi, L.Q., and Byerlee, J.D. (1982) Strain hardening and strength of clay-rich fault gouges. *Journal of Geophysical Research*, **87**, 6771–6780.

Nishimura, S., Kodama, M., Yao, K., Imai, Y., and Tateyama, H. (2002) Direct surface force measurement for synthetic smectites using the atomic force microscope. *Langmuir*, **18**, 4681–4688.

Piner, R.D., Xu, T.T., Fisher, F.T., Qiao, Y., and Ruoff, R.S. (2003) Atomic force microscopy study of clay nanoplatelets and their impurities. *Langmuir*, **19**, 7995–8001.

Price, D.G. (2009) Geological masses. Pp. 63–90 in: *Engineering Geology: Principles and Practice* (M.H. de Freitas, editor). Springer, Berlin, 460 pp.

Ruan, J.A. and Bhushan, B. (1994) Atomic-scale friction measurements using friction force microscopy. 1. General principles and new measurement techniques. *Journal of Tribology*, **116**, 378–388.

Schleicher, A.M., Warr, L.N., and van der Pluijm, B.A. (2009) On the origin of mixed-layered clay minerals from the San Andreas Fault at 2.5–3 km vertical depth (SAFOD drillhole at Parkfield, California). *Contributions to Mineralogy and Petrology*, **157**, 173–187.

Schleicher, A.M., van der Pluijm, B.A., and Warr, L.N. (2010) Nanocoatings of clay and creep of the San Andreas fault at Parkfield, California. *Geology*, **38**, 667–670.

Scholz, C.H. (1998) Earthquakes and friction laws. *Nature*, **391**, 37–41.

Selvam, A., See, C.H., Barkdoll, B., Prasad, S., and O'Haver, J. (2006) Use of atomic force microscopy for examining wet clay. *Clays and Clay Minerals*, **54**, 25–28.

Solum, J.G., Hickman, S.H., Lockner, D.A., Moore, D.E., van der Pluijm, B.A., Schleicher, A.M., and Evans, J.P. (2006) Mineralogical characterization of protolith and fault rocks from the SAFOD Main Hole. *Geophysical Research Letters*, **33**, L21314.

Solum, J.G. and van der Pluijm, B.A. (2009) Quantification of fabrics in clay gouge from the Carboneras fault, Spain and implications for fault behavior. *Tectonophysics*, **475**, 554–562.

Stiernstedt, J., Rutland, M.W., and Attard, P. (2005) A novel technique for the *in situ* calibration and measurement of friction with the atomic force microscope. *Review of Scientific Instruments*, **76**, 083710.

Svedberg, T. and Nichols, J.B. (1923) Determination of size and distribution of size of particle by centrifugal methods. *Journal of the American Chemical Society*, **45**, 2910–2917.

Tembe, S., Lockner, D.A., Solum, J.G., Morrow, C.A., Wong, T.-F., and Moore, D.E. (2006) Frictional strength of cuttings and core from SAFOD drillhole phases 1 and 2. *Geophysical Research Letters*, **33**, L23307.

Wenk, H.R., Kanitpanyacharoen, W., and Voltolini, M. (2010) Preferred orientation of phyllosilicates: Comparison of fault gouge, shale, schist. *Journal of Structural Geology*, **32**, 478–489.

Wintsch, R.P., Christoffersen, R., and Kronenberg, A.K. (1995) Fluid-rock weakening of fault zones. *Journal of Geophysical Research*, **100**, 13021–13032.

Wu, F.T., Blatter, L., and Roberson, H. (1975) Clay gouges in the San Andreas Fault System and their possible implications. *Pure and Applied Geophysics*, **113**, 87–95.

Zoback, M.D. (2000) Strength of the San Andreas. *Nature*, **405**, 31–32.

Zoback, M.D., Hickman, S., and Ellsworth, W. (2010) Scientific drilling into the San Andreas fault zone. *EOS*, **91**, 197–199.

(*Received 9 September 2010; revised 3 December 2010; Ms. 482; A.E. F. Bergaya*)